ELSEVIER

Chemical Engineering Journal 98 (2004) 219–235

Chemical Engineering Journal

www.elsevier.com/locate/cej

Experimental study of heat regimes on a dry, partially or completely wetted and liquid filled catalyst particle

V.A. Kirillov*, A.V. Kulikov, N.A. Kuzin, A.B. Shigarov

Boreskov Institute of Catalysis, Siberian Division of the Russian Academy of Science, Pr. Akad. Lavrentieva 5, 630090 Novosibirsk, Russia

Received 14 February 2003; accepted 8 August 2003

Abstract

Steady-state and dynamic-heat regimes on the dry, partially wetted, and completely filled catalyst particles were studied using the model reactions of benzene, α-methylstyrene and octene hydrogenation over the several catalysts with different porous structures, apparent catalytic activities, and heat conductivities. A rise in the particle temperature at the external limitation regime was studied and the effective diffusion coefficients of limiting species were determined.

The regime of particle preheating, gas temperature, hydrogen saturation of AMS or octene vapors, and the liquid mass flow rate on the top of a catalyst particle were varied. The phase equilibrium between the vapor saturated hydrogen and the partially wetted catalyst particle is found to essentially affect for dynamic runaway of the particle. According to the measured center and surface temperatures of each particle, there are two significantly different steady states in the range of liquid flow rates. A catalyst wetted by liquid and blown off with dry hydrogen provides a temperature hysteresis phenomenon. This phenomenon is characterized by the regime when the catalyst particle is almost liquid filled and its temperature is lower than that of gas. Another high-temperature regime occurs if a catalyst particle is almost dry and its temperature is higher than that of gas. Ignition and extinction dynamics of the catalyst particle were studied under conditions of the combined evaporation and hydrogenation processes.

Keywords: Multiphase reactions; Catalyst particle; Vaporization; Ignition; Extinction; Mathematical modeling; Mass and heat transfer

1. Introduction

A trickle-bed reactor (TBR) is a system in which gas and liquid reactants contact in a co-current down flow through a fixed bed of the heterogeneous catalyst. TBRs are widely used in petroleum, petrochemical and chemical industries for pollution abatement as well as in biochemical and electrochemical processes. These reactors usually operate under stable steady-state regimes. However, the recent operation experience and experimental data show that certain conditions provide hot spots in the trickle bed [1–5], hysteresis [6], temperature oscillations [7,8], and runaway [9,10].

The above phenomena can be caused by several reasons. The first is associated with the presence of completely filled, partially wetted and dry particles in the trickle bed [11]. Partial wetting of the catalyst particle, exothermicity of the hydrogenation reaction, resulting in the catalyst heating and evaporation of the reacting components, provide conditions for a simultaneous occurrence of the liquid-phase hydrogenation on the filled and wetted particles and the gas-phase hydrogenation on the dry catalyst particles.

Previous studies of TBRs focused mainly on the operation conditions where liquid evaporation was not important. The porous catalyst particles were considered as internally liquid filled even if they were only partially covered by liquid. However, several studies have demonstrated that the gas-phase reaction may occur under TBR conditions [1,7,12–15] whereas evaporation of the liquid phase, driven by heat generated by the exothermic reaction, may have strong influence on the heat regimes in the reactor.

It was shown that evaporation with an exothermic reaction is much faster than that without the reaction. In particular, Watson and Harold [14] found that the particle drying accompanied by the reaction of cyclohexene hydrogenation is almost 5-fold faster than drying without a reaction. An increase in the vaporization rate may result in a partially wetted and filled catalyst in which both the gas and liquid-phase reactions occur as well as in a completely dry particle in which only the gas-phase catalytic reaction occurs. The external and internal drying of the catalyst inevitably leads to a change of the apparent reaction rate, which, in turn, influences the evaporation rate. Such interplay between the

* Corresponding author. Tel./fax: +7-3832-34-11-87.
E-mail address: v.a.kirillov@catalysis.nsk.su (V.A. Kirillov).

1385-8947/$ – see front matter © 2003 Elsevier B.V. All rights reserved.
doi:10.1016/S1385-8947(03)00250-X

Nomenclature

C	AMS molar fraction in the liquid phase
C_p	heat conductivity (J/mol K)
d	diameter of a catalyst particle (mm)
D	diffusion coefficient (m^2/s)
D_{ij}	binary diffusion coefficient (m^2/s)
D_0	effective diffusion coefficient of the limiting component (m^2/s)
E	energy activation (J/mol)
f	wetted area fraction of the particle
G	mass flow rate of the liquid hydrocarbon onto the top of a catalyst particle (g/s)
H	heat of evaporation (J/mol)
K_0	constant of the reaction (mol/m^2 s)
M	molar mass (g/mol)
P	atmospheric pressure (Pa)
P^*	10^{10} Pa
Q	heat of the reaction (J/mol)
R	universal gas constant (8.31 J/mol K)
S	external surface of the particle (m^2)
T	temperature (°C)
T_0	bulk gas temperature (°C)
T_1	temperature in the center of a catalyst particle (°C)
T_2	axial temperature of the catalyst particle (°C)
ΔT	temperature difference
U	gas velocity (m/s)
W	rate of evaporation (g/s)
x	mole fraction of hydrocarbon

Greek letters

α	heat transfer coefficient (W/m^2 K)
β	mass transfer coefficient (m/s)
γ	the ratio between the liquid mass flow rate and the liquid vaporization rate
δ	the ratio between the heat generation of the chemical reaction and the convective heat removal from the particle surface
η	efficiency of the catalyst particle
λ	heat conduction of the gas mixture (W/m K)
λ_P	heat conduction of the catalyst particle (W/m K)
Λ	the ratio between the liquid evaporation heat and the convective heat removal from the particle surface
μ	dynamic viscosity (N s/m^2)
ρ	molar density (mol/m^3)
ρ_m	mass density (kg/m^3)
χ	the ratio between the rate of chemical reaction and the rate of liquid vaporization

Subscripts/superscripts

A	hydrogenate species
AB	AMS–cumene (octane–octane)
AH	AMS–hydrogen (octane–hydrogen)
AMS	α-methylstyrene
B	hydrogenate product
BEN	benzene
BH	cumene–hydrogen (octane–hydrogen)
cum	cumene
dry	dry surface of the particle
H	hydrogen
int	into porous particle
oct	octene
tot	total hydrocarbon mass flow rate
wet	wetted surface of the particle
x	critical value
0	bulk
$*$	equilibrium value

exothermic reaction and phase transition processes can result in a number of steady states of the catalytic particle containing different parts of the dry external and internal surfaces [16]. An attempt to present a mathematical description of the above phenomena is given in [17,18].

Since the rate of mass transport is higher in a gaseous system and heat removal is less effective, the overall reaction rate in a partially or completely dry catalyst can be significantly higher than that in the completely wetted catalyst. In particular, Watson and Harold [15] observed that the rate of cyclohexene hydrogenation increased by about 20 times for the same bulk conditions if drying is induced in the catalyst pores.

At present there is an obvious progress in understanding the role of phase transition processes in TBR, however, experimental data are obtained only for the restricted range of the operating conditions and systems.

The evaporated components of the liquid phase react with hydrogen on the dry catalyst surface. When the catalyst activity is rather high and the concentration of evaporated species is also high, hydrogenation in the gas phase may proceed by the external diffusion control. This is extremely undesired for the process conditions, because the external diffusion limitation causes an essential excess of the catalyst temperature and may provide formation of hot spots in the trickle bed.

There are few experimental studies on the gas-phase heterogeneous reactions involving hydrogen, which occur on the catalyst particle at the external diffusion regime. Thus [19], the reaction of hydrogen oxidation was experimentally studied on the platinum wire at the external mass transfer limitation. The dynamics of the reaction ignition on the catalyst particle 17–30 mm in size was studied on the hydrogen oxidation in [20]. It was found that the particle ignition starts on the particular surface parts where mass transfer is higher. The rate of cyclohexane dehydrogenation governed by external diffusion was experimentally studied in [21].

Since the amount of the experimental data on the regulations of hydrogenation performance in the external diffusion

region is not sufficient, it is necessary to provide additional investigations. The goals of the present study are to experimentally examine heat regimes on the dry, partially wetted and liquid filled catalyst particles in the exothermic reaction of hydrocarbon hydrogenation and elucidate the combined effect of the exothermic chemical reaction and phase transition on the steady-state and dynamic-heat regimes of catalytic particles.

2. Experimental setup and procedure

The experimental setup used to study particle heat regimes consists of a single particle reactor (SPR) with a gas saturator, air heaters, liquid and gas supplying systems, and control and monitoring devices. The main parts of this installation are presented in Fig. 1 and were similar to that employed in [16]. In contrast to the reactors used by Funk et al. [11] and Watson and Harold [14,15], the experimental reactor was horizontally placed and equipped with a gas saturator for evaporating and premixing of liquid reagents with the gas phase entering the reactor. The saturator and SPR were connected together. Heating and evaporating of the liquid on the surface of electrically heated metallic packing in the saturator result in the formation of different fractions of the evaporating reagent in the gas phase supplied to the reactor. The saturator and SPR contained a Pyrex glass cylinder (15 mm i.d.) and were surrounded with an annular glass hot air jacket to provide an isothermal environment. A cylindrical catalytic particle was placed in the middle of the reactor in the vertical position.

The setup was used for:

1. Gas-phase experiments: during these runs a catalyst particle is completely dry. Hydrogen and hydrocarbon vapor from the saturator are fed to SPR and blown off the particle. Hydrogenation proceeds only in the gas phase on the catalyst particle and liquid is not fed on the particle top.

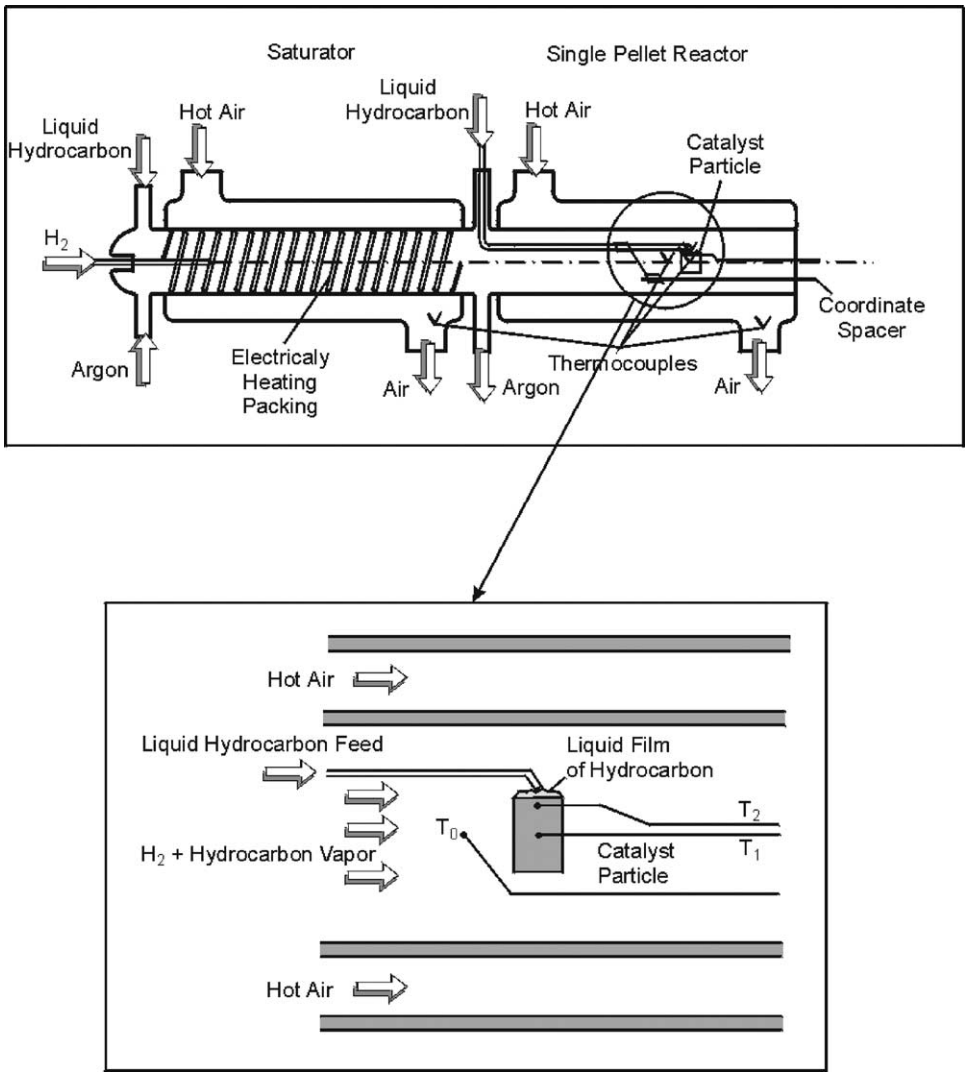

Fig. 1. Principal scheme of the experimental setup.

2. Experiments with a partially wetted and filled catalyst particle: in these experiments, liquid is supplied onto the particle top and particle blows off hydrogen and hydrocarbon vapor. Hydrogenation between the hydrocarbon and hydrogen in gas phase and hydrogen dissolved in the liquid phase proceeds on the catalyst particle.

For the second case, the steady-state and dynamic experiments were performed. In these runs, the liquid reagent was fed to the top of the catalytic particle through a stainless tube (1 mm i.d.) fitted with a glass capillary (0.2 mm i.d.) at its end. The diameter and length of the small tube inside the reactor ensured similar temperatures of liquid feeding and the bulk. The detailed schemes of the central part of the reactor and a temperature monitoring are shown in Fig. 1. Two thermocouples 0.2 mm in diameter were carefully implanted into the particle. One thermocouple measured temperature T_1 in the center of the particle and the other measured subsurface temperature T_2 at a certain distance from the top. The thermocouples were sufficiently rigid to hold the particles in a fixed position.

Two series of the steady-state experiments were performed. The first series was devoted to study the temperature distribution along the particle axis. The second series was aimed at studying the influence of the experimental conditions on temperature in the particle center and at a distance of 0.8 mm from the top face. To measure the axial temperature distribution along the cylinder catalyst particle in the starting experiment, the thermocouple was inserted along the axis to a depth of 1.8 mm from the top face to measure T_2. Then the particle face was ground off by 0.3–0.5 mm and the next experiment was performed. This procedure was repeated for several times until the thermocouple reached the catalyst particle top.

In these experiments we applied two methods to implant a thermocouple to measure T_2 in the particle. According to the first method, a catalyst particle was drilled from the generatrix towards the center and the thermocouple was inserted tightly into the hole. For the other method, a thermocouple was implanted into a gash 1.8 mm in depth made on the particle face, and sealed with the catalyst-containing composite. The temperatures plotted vs. thermocouple coordinates allowed us to estimate the temperature profile along the catalyst particle axis. In all experiments, the top face of the catalytic particle was assumed to be the zero point of the axis coordinate; the catalytic particle was 4.8 mm in diameter and the initial height was 6.4 mm. As follows from the above experiments, both methods of the thermocouple arrangement produced similar results. Gas temperature (T_0) was measured with a moveable thermocouple, which provided temperature measurements at any point in the reactor (Fig. 1).

For the experimental study of heat regimes, the following exothermic reactions were used:

- Hydrogenation of α-methylstyrene (AMS) to cumene:

$$C_9H_{10} + H_2 = C_9H_{12} + 109\,kJ/mol$$

- Hydrogenation of octene to octane:

$$C_8H_{16} + H_2 = C_8H_{18} + 125\,kJ/mol$$

- Hydrogenation of benzene to cyclohexane

$$C_6H_6 + 3H_2 = C_6H_{12} + 216\,kJ/mol$$

3. Characterization of catalysts and experimental conditions

We used several types of catalysts supported on γ-Al_2O_3, Sibunit (carbon material) and Ti–Al. The catalysts have a different porous structure, distribution of the active component (Pt, Pd) and heat conductivity. Pt-based catalysts were prepared by impregnating the γ-Al_2O_3 support with an aqueous solution of platinum hydrochloric acid. After impregnation, the catalyst was dried at 120 °C in nitrogen and heated at 250 °C. The catalyst was reduced in a nitrogen–hydrogen (hydrogen 10–15 wt.%) mixture at 350 °C for 1 h and cooled to 50 °C. Pt content in the catalyst was determined by X-ray fluorescence analysis using a VRA-20 analyzer with a W-anode in the X-ray tube. The specific surface area of the support and the total surface of the catalyst were determined by the BET method using the argon heat desorption. The surface of metallic palladium was determined by oxygen pulse chemisorption at room temperature. The total pore volume of samples and the radius pore distribution were determined by mercury porosimetry using a "Pore Sizer 9300" porosimeter. Some properties of the γ-Al_2O_3 support and the related catalysts are given in Table 1. Using a 15% Pt/γ-Al_2O_3 base we have prepared three catalyst versions, which differ by the active component distribution regarding the particle radius. In the first type catalyst, the active component is uniformly distributed along the particle radius, and in the second catalyst version (egg-shell catalyst), the active component Pt/γ-Al_2O_3 is primarily situated in the layer 0.7 mm in width near the particle surface. The residue volume is filled by γ-Al_2O_3. For the third version, an inactive layer of γ-Al_2O_3 enclosed the active component situated in the central part of the particle (egg-yolk catalyst).

A sample of the Pd catalyst supported on the porous Ti–Al material was prepared by sintering a mixture of metallic titanium (62.5 wt.%) and aluminum (37.5 wt.%). After heating at 600 °C in hydrogen, the support specific surface is ∼0.1 m^2/g and the total specific pore volume is ∼0.26 cm^3/g. The X-ray phase analysis exhibits the presence of the following phases: AlTi, Al_3Ti, $AlTi_3$, and Ti. In order to increase the specific surface area, the carrier was covered with an additional alumina support (∼10 wt.%) via the aluminum nitrate impregnation and heating at 550 °C in nitrogen flows. According to the scanning electron microscopy, the initial support consists of conglomerates ∼7–10 μm in size formed

Table 1
Properties of the supports and catalysts used in the experiments

Support properties				Catalyst properties					
S_{sp} (m^2/g)	Volume of pores of radius Å (cm^3/g)			Active component concentration (mass%)	S_{sp} (m^2/g_{cat})	Size of active component (Å)	Volume of pores of radius Å (cm^3/g)		
	<40*	40–10^3	>10^3				<40*	40–10^3	>10^3
γ-Al_2O_3 support and Pt/γ-Al_2O_3 catalyst									
220	0.09	0.50	0.17	Pt = 15.2	206	18	0	0.45	0.20
	<10^2	10^2–10^5	>10^5				<10^2	10^2–10^5	>10^5
Ti–Al support and Pd/Ti–Al catalyst									
10	0	0.06	0.12	3.5	9	500	0	0.053	0.068

Table 2
Operation conditions in the gas-phase experiments (the reactor is 15 mm in diameter and the particle is 4–4.5 mm in size)

Reaction of hydrogenation	Catalyst	Gas temperature (°C)	Molar fraction of hydrocarbons	Hydrogen flow velocity (cm^3/s)
AMS	3.5% Pd/Al_2O_3, 15% Pt/Al_2O_3	140–190	0.1–0.9	2–250
AMS–cumene 1:2	3.5% Pd/Al_2O_3, 15% Pt/Al_2O_3	170–175	0.04–0.303	2–181
Octene	3.5% Pd/Al_2O_3	120–140	0.05–0.62	2–175
AMS–octene 1:1	3.5% Pd/Al_2O_3	123–128	0.1–0.6	5–76
Benzene	15% Pt/Al_2O_3	20–360	0.07–0.3	31–118
AMS–benzene 1:1	15% Pt/Al_2O_3	100–136	0.1	5–66
Benzene–octene 1:1	15% Pt/Al_2O_3	48–371	0.1–0.2	26–58

by the intergrowth of granules ~2 μm in size. The properties of the support used for preparation of palladium catalysts are listed in Table 1. The porous structure of the support and the catalyst is characterized by a small total pore volume (<0.2 cm^3/g) and the presence of big pores: the main pore volume is formed by pores of radius ranging from 100 000 to 300 000 Å; the volume of the pores of a radius less than 10 Å is not more than 0.01 cm^3/g. The data on the X-ray line breadth indicate that the size of particles in the supported palladium is ~500 Å. Along with the Pd/Ti–Al catalyst, we used a 0.5% Pd supported on the Sibunit (porous carbon support) catalyst. This catalyst is characterized by a wide-porous structure, high heat conductivity and better wettability of the porous structure compared to the γ-Al_2O_3 support. Tables 2 and 3 summarize all experimental conditions used in the experiments on the gas phase, partially wetted and liquid filled particles.

4. Experimental results

4.1. Gas-phase experiments

For the chosen experimental conditions of AMS and octene hydrogenation, the rate of gas flow does not affect the particle temperature difference $\Delta T = T_1 - T_0$ starting from Reynolds number >50. Also the influence of the bulk temperature on the particle temperature difference is not significant. This indicates that reaction occurs at the external mass transfer limitation.

On the benzene hydrogenation, the effect of the bulk temperature on the particle temperature is rather complex (see Fig. 2). Thus, when the bulk temperature is low, x^0_{BEN} raises significantly the particle temperature. As T_0 increases further, the results obtained for all concentrations approach each other and the particle and bulk temperature completely

Table 3
Operating conditions in the experiments with partially wetted and liquid filled particles (the diameter of the reactor is 15 mm and the hydrogen mass flow rate is 18.5 cm^3/s)

Reaction of hydrogenation	Catalyst	Size of particle (mm)	Gas temperature (°C)	Molar fraction of hydro carbon	Liquid mass flow rate (g/s)
AMS	15% Pt/Al_2O_3	4.8 × 5.7	86–135	0.10–0.50	0–16 × 10^{-4}
AMS	15% Pt/Al_2O_3, egg-shell	5.2 × 6.6	135	0.46	0–15.1 × 10^{-4}
AMS	15% Pt/Al_2O_3, egg yolk	5.2 × 6.6	135	0.46	0–14 × 10^{-4}
AMS	0.5% Pd Sibunit	4.5 × 4.5	127–136	0.30–0.46	0–18.6 × 10^{-4}
AMS	3.5% Pd/Ti–Al	4.8 × 6.5	126–136	0.30–0.46	0–21.9 × 10^{-4}
Octene	15% Pt/Al_2O_3	4.8 × 5.7	105–115	0.16–0.31	0–43 × 10^{-4}

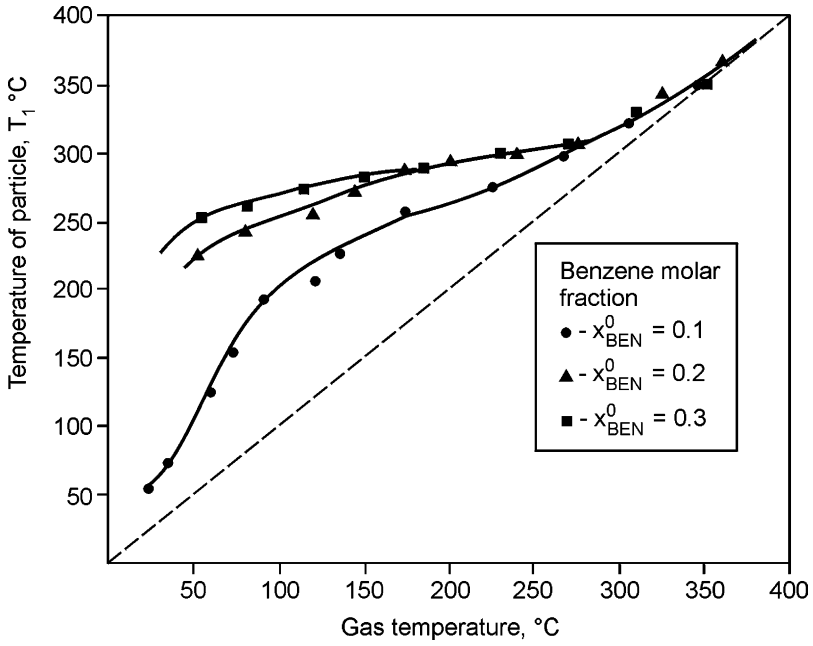

Fig. 2. Impact of the bulk temperature and the benzene molar fraction on the catalyst particle temperature on benzene hydrogenation. Conditions: catalyst 15% Pt/Al_2O_3; hydrogen flow velocity 78.3 cm^3/s ($x^0_{BEN} = 0.1$), 34.8 cm^3/s ($x^0_{BEN} = 0.2$), 20.3 cm^3/s ($x^0_{BEN} = 0.3$).

coincide at $T_1 > 250\,^{\circ}C$. The experimental conditions and results were described in more detail elsewhere [22]. Such evolution of the particle temperature is caused by the reaction proceeding in the transient region and the reaction kinetics, which provide the extreme dependence between reaction rate and increasing catalyst temperature [23] as well as by the reverse reaction contribution at $T_1 > 250\,^{\circ}C$.

Fig. 3 shows the impact of AMS molar fraction on the particle temperature difference on AMS hydrogenation. As AMS concentration in the bulk is at almost constant T_0, ΔT reaches its maximum value $x^0_{AMS} = 0.6$–0.65. When x^0_{AMS} is higher, ΔT decreases.

The experimental points related to the particle temperature difference lie between two curves. The upper curve corresponds to the results obtained on the fresh catalyst. The lower curve shows the data obtained on the catalyst particle after a series of experiments. Note that the system transition from the upper to the lower curve is rather fast. One may follow how ΔT decreases at $G_{AMS} = 0.105$ g/s during four sequential cycles. In each cycle, a decrease in the rate of hydrogen supply from 181 to 2.2 cm^3/s and its following increase to the initial value provided a change in the AMS concentration in gas. The system proceeds along the whole curve for approximately 40 min.

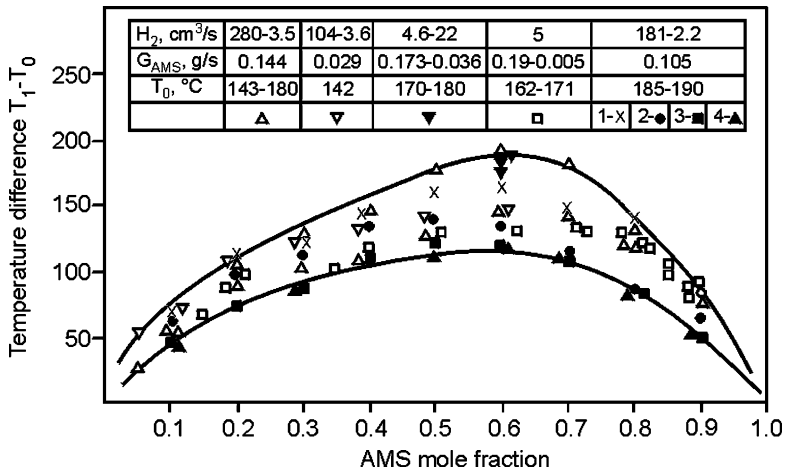

Fig. 3. Experimentally measured difference of the particle temperature in the AMS hydrogenation, catalyst 15% Pt/Al_2O_3.

It was found experimentally that the effect of a decrease in the catalyst particle temperature difference depends on the run duration (especially for high vapor fractions), which is probably associated with the AMS polymerization resulting in a partial blocking of the particle surface. The experiments on the gas-phase hydrogenation confirm this hypothesis [1].

The addition of cumene into the AMS–hydrogen mixture does not change the general picture, but decreases the molar fraction of AMS in the mixture and thus decreases the temperature difference.

In actual industry, one usually deals with hydrogenation of hydrocarbon mixtures. Therefore, it is reasonable to experimentally determine the effect of mixture composition on overheating of the catalyst particle during performance of several hydrogenation reactions in the external diffusion limitation regime. Fig. 4 demonstrates the difference of the catalyst particle temperature on hydrogenation of octene or its mixtures (octene–AMS, octene–benzene) and the summary concentration of hydrocarbons in the gas along the horizontal axis. Because of the similar heat of reaction, the experimental data on the octene hydrogenation are close to that obtained for the AMS hydrogenation. An addition of benzene to octene decreases the general temperature difference of the catalyst particle. Therefore, Figs. 2–4 show an intriguing effect of the gas-phase hydrogenation reaction of AMS, octene and benzene under external mass transfer limitation.

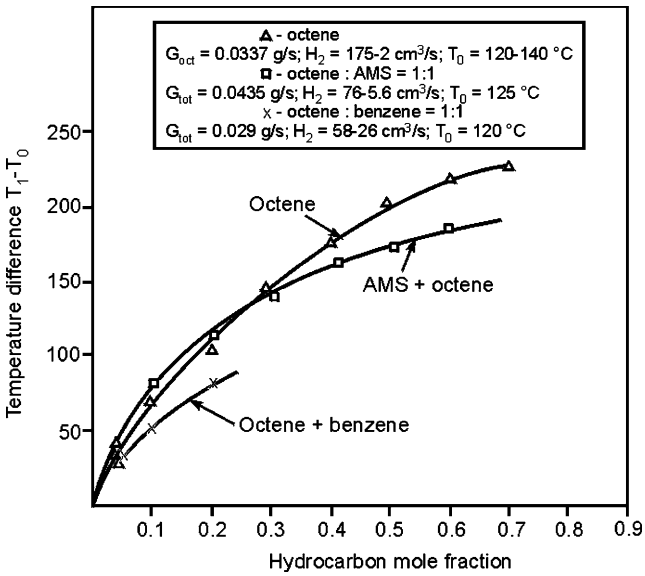

Fig. 4. Experimentally measured difference of the particle temperature on the hydrogenation of octene and its mixtures with AMS and benzene, catalyst 15% Pt/Al_2O_3.

4.2. Experiments with presaturated hydrogen

Fig. 5 presents the experimental data of the axial temperature distribution along a cylinder catalyst particle treated with AMS vapor saturated hydrogen and liquid AMS, which was fed on the particle top. The experiments were performed using several particles with 15% Pt/γ-Al_2O_3 and a uniform distribution of the active component into the catalyst particle. As Fig. 5 suggests, the catalyst particle is practically isothermal on the gas-phase hydrogenation if liquid AMS is not fed on its face. An insignificant temperature decrease

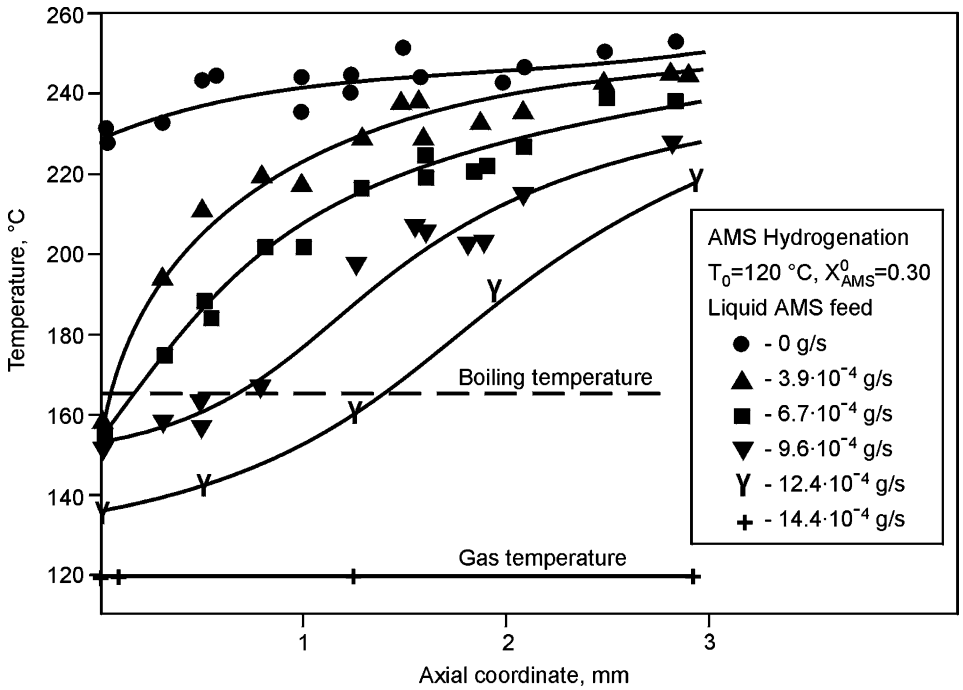

Fig. 5. Impact of AMS liquid feeding on the axial temperature distribution into the catalyst particle, catalyst 15% Pt/Al_2O_3 with uniform active component distribution.

near the top face may be attributed to heat losses through the thermocouples.

As AMS was fed at 3.9×10^{-4} g/s, the top face temperature sharply decreased from 230 °C (gas-phase regime) to 157 °C, i.e. below the AMS boiling point. Due to low heat conductivity of the particle, the center temperature is much higher than that of the wetted surface. A further increase in the rate of AMS feeding decreases the wetted surface temperature to T_0. If the AMS flow rate is below 12.4×10^{-4} g/s, the liquid boiling point is attained at a distance of 0.2–1.2 mm from the top face. This means that the external surface of the particle is partially wetted and filled with liquid to this thickness and the remaining particle volume is filled with gas. However, an insignificant increase in the rate of AMS flow from 12.4×10^{-4} to 14.4×10^{-4} g/s provides a complete filling of the particle.

A significant influence of vaporization has been established using the feeding of liquid cumene on the face of a particle blown off with AMS-saturated hydrogen (Fig. 6). If the rate of cumene feed exceeds 9.6×10^{-4} g/s, the particle temperature decreases below the gas bulk temperature owing to the intense vaporization. A comparison of Figs. 5 and 6 shows a decrease in the particle temperature in the experiments with AMS vaporization was less significant than that in experiments with cumene. To provide complete particle filling, the rate of AMS feeding should be higher than that of cumene by a factor of 1.5.

The impact of liquid flow rate, catalyst particle heat conductivity, gas temperature and active component distribution on temperature difference $(T_1 - T_0)$ for AMS and octene hydrogenation is presented in Fig. 7. Varying the gas temperature and increasing the rate of liquid AMS flow on the catalyst pellet, it is possible to obtain two different dependencies of ΔT vs. G_{AMS}. Thus, if temperature ($T_0 = 69$ °C) is significantly lower than the boiling temperature of liquid, i.e. the concentration of AMS vapor in gas is not high, an increase in G_{AMS} at low liquid flow rates provides an increase in the pellet overheating. This phenomenon may be caused by evaporation of the liquid penetrated into the particle and reaction of the formed AMS vapors in the porous structure. As ΔT reaches some maximal value, a further increase in AMS flow rate provides a drastic decrease in pellet overheating, which is probably associated with liquid filling of porous structure.

There are two steady-state regimes for catalyst particle if gas temperature $T_0 = 125$ °C. When the catalysts are in the upper steady state and the liquid flow rates do not exceed the certain critical values, the catalyst temperatures gradually decrease as the liquid supply increases. A slow decrease in the temperatures along the upper branches can be attributed to heat consumptions required for heating and evaporation of the increasing amounts of fed liquid. In all experiments, the center temperature of catalyst with uniform and egg-shell active component distribution on the upper branches is considerably higher than the boiling point of liquid hydrocarbon. When the rates of liquid feeding exceed the critical value, G^x_{AMS}, the particle temperature sharply decreases to the value, which is practically equal to gas temperature. The steady state of the catalyst particle changed from the gas filled state to the completely liquid filled state. A further

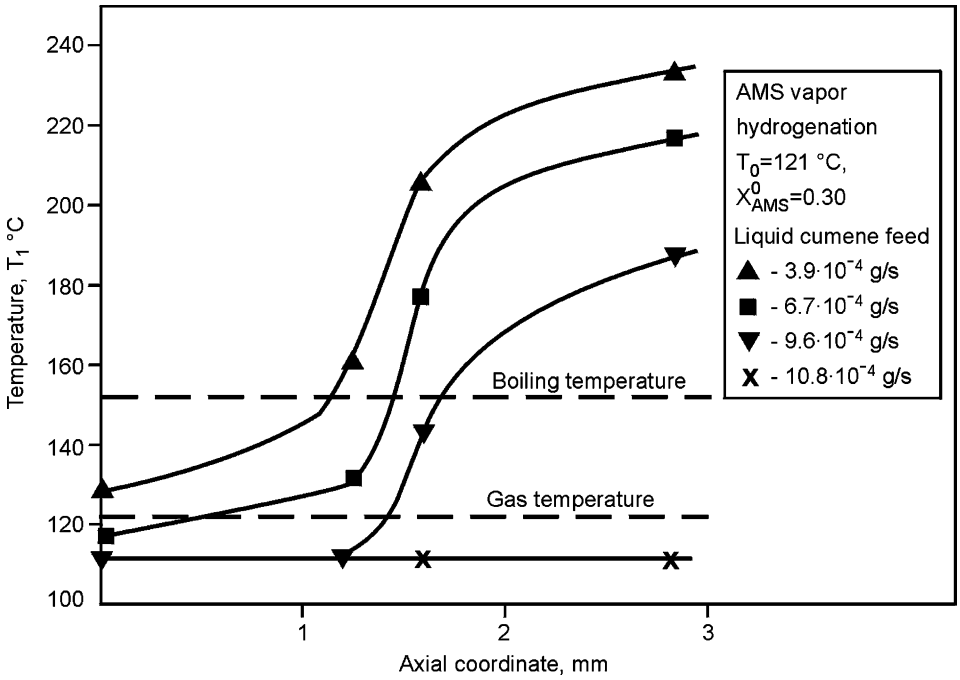

Fig. 6. Impact of the cumene liquid feeding on the axial temperature distribution into the catalyst particle, catalyst 15% Pt/Al_2O_3 with uniform active component distribution. Hydrogen flow rate is 18.5 cm^3/s.

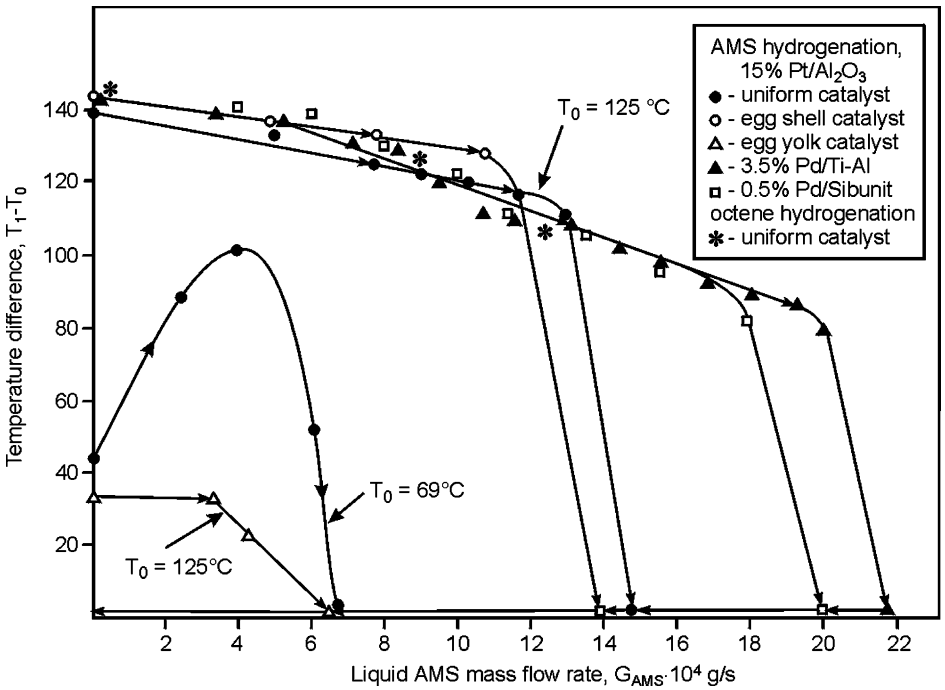

Fig. 7. Impact of the AMS liquid mass flow rate and particle properties on the heat steady-state regime of the catalyst particles for hydrogenation of H_2 saturated with AMS. Hydrogen flow rate is 18.5 cm^3/s.

increase (or decrease) in the liquid flow rate does not influence the catalyst temperatures. The catalysts remained internally fully filled. Even if the liquid supply decreased to zero ($G_{AMS} = 0$), the particle temperature did not change for at least 30 min. This means that if the gas phase is completely saturated with AMS the pores of the particles are filled with liquid even without liquid feeding.

The obtained data show that the particles with uniform or egg-shell distributions of the active component exhibit practically the same behavior if gas temperature $T_0 = 125\,^{\circ}C$. For the egg-yolk type catalyst, particle–gas temperature difference $T_1 - T_0$ and the critical liquid flow rate are much lower than for the other catalysts. This can be attributed to the internal diffusion resistance in the catalytically inactive layer of the egg-yolk catalyst.

Fig. 8 illustrates the steady-state regimes at gas temperatures of 125, 132 and 143 °C for $x^0_{AMS} = 0.30$ and at $T_0 = 132\,^{\circ}C$ for $x^0_{AMS} = 0.41$. For $G_{AMS} = 0$, an increase in the gas temperature at a constant molar fraction of AMS does not affect the temperature difference. This indicates the external diffusion limitation of the AMS gas-phase hydrogenation in high-temperature steady-state regime. For the non-equilibrium condition, liquid evaporates from the external wetted surface of the particle to unsaturated gas and the critical flow rate of liquid increases when hydrogen saturation decreases. For the low steady-state regime the particle temperature in this case is lower than the gas temperature by 10 °C. Such steady-state regime is stable till the AMS flow rate decreases to 3×10^{-4} g/s. In contrast to the saturated gas, a further decrease in G_{AMS} results in the temperature increase by 130 °C, and the reaction transition to the high-temperature regime.

The low-temperature steady state is rather sensitive to a deviation from the vapor–liquid equilibrium. The sensitivity increases with decreasing liquid flow rates. The reaction transfers from the lower to the upper branch at $G_{AMS} = 0$, if the gas composition is slightly disturbed from the phase equilibrium state.

Fig. 9 illustrates this phenomenon for the cases when gas temperature and hydrogen saturation have deviations from the preliminary phase equilibrium state. The arrows in this figure indicate the direction of temperature variations. In the first run (points 1, 2, 3, 4) the low-temperature steady state (the lower branch in Fig. 7), was attained for the gas phase consisting of hydrogen and saturated AMS vapor (point 1 in Fig. 9) at a gas temperature of 106 °C. Then the gas temperature was increased to 108 °C with no changes in the gas-phase composition. As a result, there is no more phase equilibrium at point 2 in Fig. 9 because of new temperature corresponds to increasing of equilibrium AMS molar fraction in hydrogen from 0.17 to 0.19. The reaction transfers to the gas-phase regime within a few minutes, which increases the particle temperature from 108 to 190 °C (point 3 in Fig. 9).

In the second run, the starting steady-state regime corresponds to the completely filled particle at a gas temperature of 115 °C (point 1′, Fig. 9). Then the gas temperature was reduced to 105 °C (point 2′) and the AMS vapor mole frac-

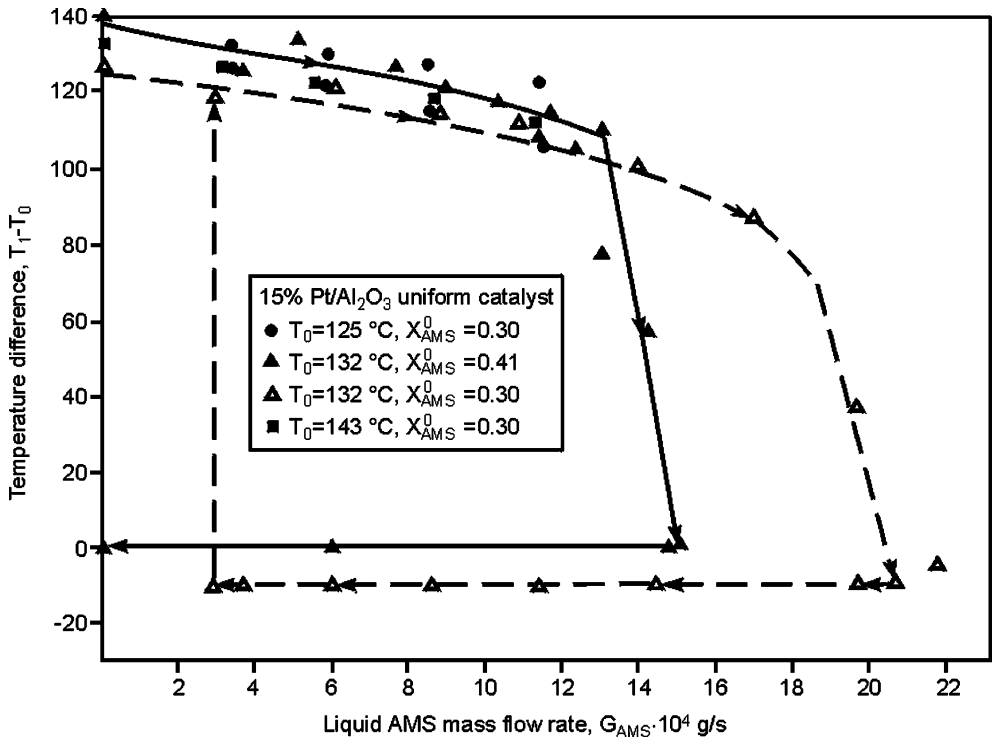

Fig. 8. Impact of the AMS liquid mass flow rate and hydrogen saturation on the heat steady-state regime of the catalyst particle. Continuous line: $T_0 = 125\,^\circ$C ($x^0_{AMS} = 0.30$), $T_0 = 132\,^\circ$C ($x^0_{AMS} = 0.41$), $T_0 = 143\,^\circ$C ($x^0_{AMS} = 0.30$); dotted line $T_0 = 132\,^\circ$C ($x^0_{AMS} = 0.30$). Hydrogen flow rate is 18.5 cm^3/s.

tion was decreased from 0.22 to 0.14. The equilibrium AMS fraction in the gas phase corresponds to 0.16 at 105 °C. As a result, the particle temperature increases from 105 to 178 °C (point 3′). Points 3, 3′ and 4 in this figure correspond to the external diffusion hydrogenation of AMS vapor.

4.3. Experiments with dry hydrogen

The experiments with dry hydrogen were performed similarly to the experiments with the presaturated hydrogen. Fig. 10 shows the center temperatures of the particles and

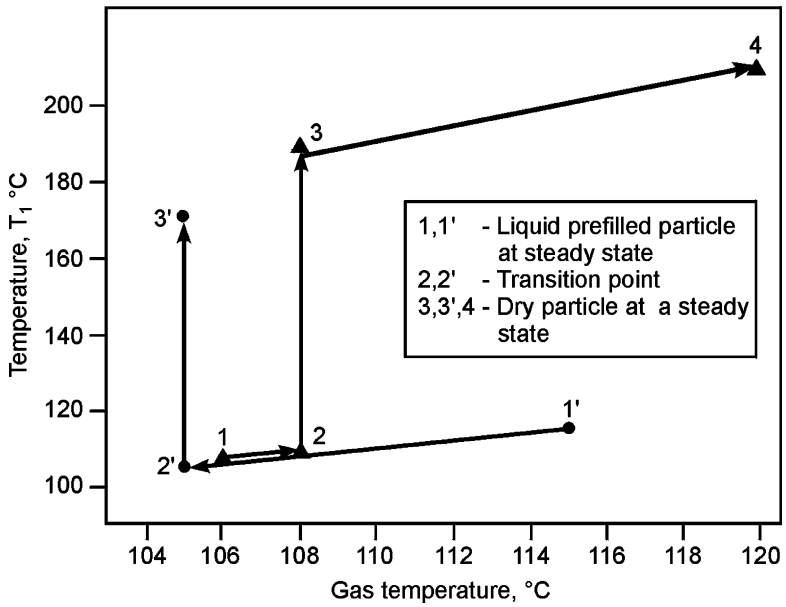

Fig. 9. Influence of the deviations from the gas–liquid equilibrium on the particle ignition on the AMS hydrogenation. Condition: catalyst 15% Pt/Al_2O_3 with uniform active component distribution, hydrogen flow rate is 18.5 cm^3/s.

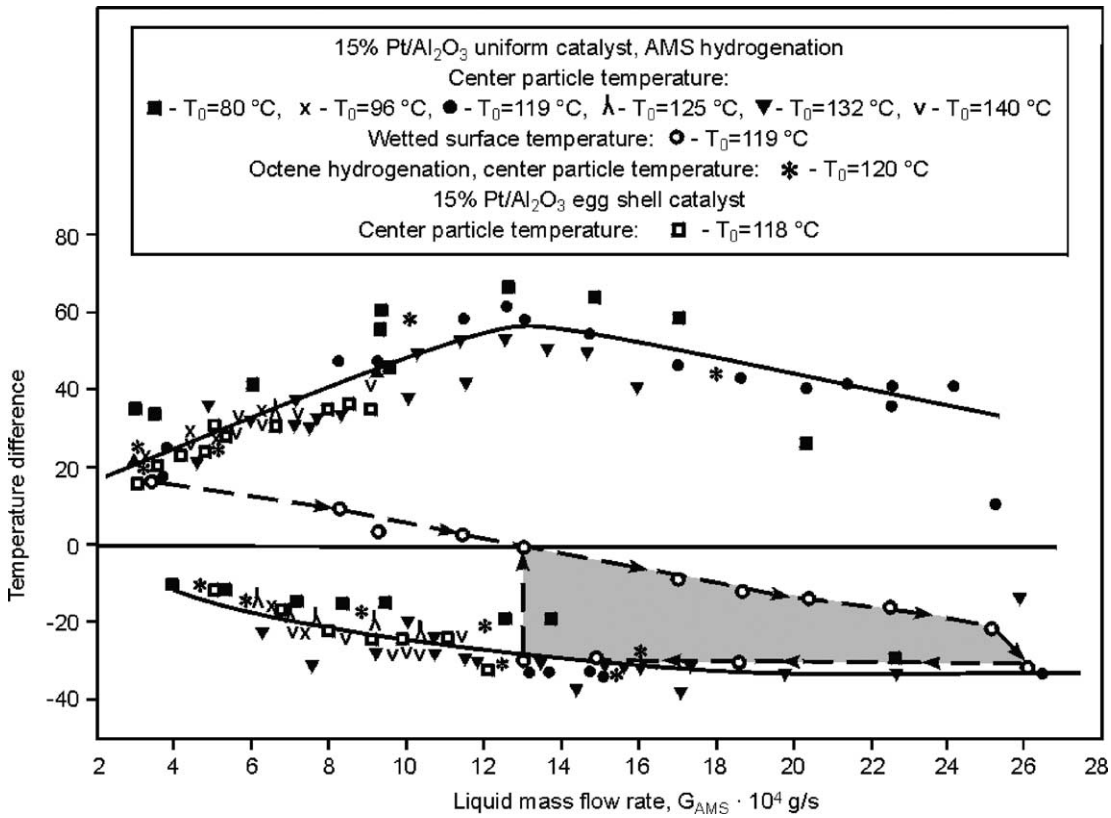

Fig. 10. Hysteresis phenomena on the filled and partially wetted catalyst particles. Catalyst—15% Pt/Al_2O_3 with uniform and egg-shell active component distributions, the shaded area is wetted surface temperature hysteresis, hydrogen flow rate 18.5 cm^3/s.

different gas temperatures in the experiments with dry hydrogen and the wetted surface temperature for a gas temperature of 119 °C. In these runs we used a 15% Pt/Al_2O_3 catalyst with the uniform and egg-shell distributions of Pt.

As in the case with the saturated hydrogen, two steady states exist for the certain ranges of the liquid flow rates. Since the experimental studying of hysteresis phenomena on a catalyst particle is always a rather complex problem, the more precise experiments were performed at a gas temperature of 119 °C. After recording 3–4 points, the catalyst particle was regenerated and its apparent activity tested. The arrows in Fig. 10 indicate the direction of variations of the AMS mass flow rate. For the other temperatures shown in Fig. 10, the catalyst was regenerated before transition to a new gas temperature level. In contrast to the unregenerated catalyst, the discrepancy of mass flow rates of liquid AMS in the critical points of the regenerated catalyst shows that the apparent catalyst activity strongly affects the particle runaway.

The region between the upper and lower branches corresponds to the unstable steady-state regimes and hysteresis phenomena; the shaded area characterizes temperature hysteresis of the particle-wetted surface. Fig. 10 shows that a change of pure hydrogen to the presaturated hydrogen causes a significant change in the steady-state behavior of the particles. The temperature of the particles exceeds that of gas by 20–60 °C and is much lower than the temperatures of the same particles in the experiments with the presaturated hydrogen. This difference in the temperatures is probably caused by evaporation of AMS from the particles, because the gas fed to the reactor does not contain AMS and hydrogen carries away the evaporated AMS. It should be noted that the center temperature of the particles on the upper branches rises as the liquid flow rate increases in a range of $(2–13) \times 10^{-4}$ g/s. This can be attributed to higher concentrations of the evaporated AMS in the gas phase.

The temperature of the particle surface at which the liquid is constantly fed decreases and attains the gas temperature at $G_{AMS} = 13 \times 10^{-4}$ g/s. A further increase in the liquid flow rate shifts the intensive vaporization into the porous structure. As a result, the surface temperature falls below the gas temperature. The temperature difference between the particle center and the wetted surface reaches 60 °C, which is in good agreement with the data on the saturated hydrogen experiments (Fig. 5).

According to the visual observation, the particles in the low-temperature steady states are almost completely wetted and their temperatures are lower than the gas temperature by 20–30 °C. These low temperatures of the particles can be explained by an intensive evaporation of AMS from the external particle surface in pure hydrogen due to a significant deviation from the vapor–liquid equilibrium. When the

liquid feed rate is reduced, liquid evaporation gives favorable conditions for partially wetting of the catalyst particle. Gas-phase reaction starts on the formed non-wetted surface and offers to intensive particle drying and temperature increasing. Particle temperature reached the ignition point, at which it abruptly shifted to the dry, high-rate branch. At this point drying begins to move into the catalyst. The ignition points in the low-temperature steady states depend on the catalyst activity. This result will be discussed below.

4.4. Dynamic experiments

The dynamic experiments were undertaken to study drying with hydrogenation of the partially or completely wetted catalyst particle blown by dry or partially saturated hydrogen in reactions of the octene and AMS gas-phase hydrogenation.

Temperature dynamics of the particle exposed to dry hydrogen after cutting off the liquid feeding and transition dynamics from the lower temperature to the upper temperature steady-state branch are shown in Fig. 11. This experiment simulates a sudden drop of the liquid flow in the reactor. At the starting point in experiment when G_{AMS} decreases from 0.00131 g/s to 0, the particle and gas temperatures were 90 and 112 °C, respectively.

After a short period, required for generating some dry area, the catalytic particle undergoes rapid ignition, and its temperature increased from 90 to 135–145 °C. Temperature passed a maximum and began to decrease, because the liquid content in the particle and the rates of AMS evaporation and reaction began to decrease. The similar particle behavior was observed by Watson and Harold [14] who found that a particle preliminary filled with cyclohexene and then exposed to pure hydrogen exhibits a temperature rise of nearly 100 °C and a rapid drying during several minutes.

Fig. 11 illustrates the transition dynamics of the liquid filled catalyst particle in the lower temperature steady-state branch associated with a decrease in the flow rate from 0.0131 to 0.00125 g/s. At the starting point, the particle and gas temperatures were 90 and 118 °C, respectively. The dynamics of such transient regime is governed by the ratio between hydrogenation and vaporization rates in the porous structure of the catalyst particle. In this regard, the dynamics is accompanied by the considerable temperature gradients. The time of the transient regime is 60 s. At the new steady-state regime, the temperature in the particle rises to 172 °C, and the temperature of the wetted surface rises to 130 °C.

In the recent study [16], the filling dynamics of the catalyst particle fed with liquid and blown off with the partially saturated hydrogen has been studied on the AMS hydrogenation when the starting temperature of the particle was higher than the boiling temperature. Here we consider the regime when the particle temperature is equal or lower than the liquid boiling temperature. The results for the dynamic ignition and extinction of the particle in the reaction of octene hydrogenation are given in Fig. 12. The time of the transient regime is determined by the ratio between the rates of particle impregnation and liquid vaporization. For the filling experiment, the particle was blown off with hydrogen and octene vapor at the starting moment. Liquid was not

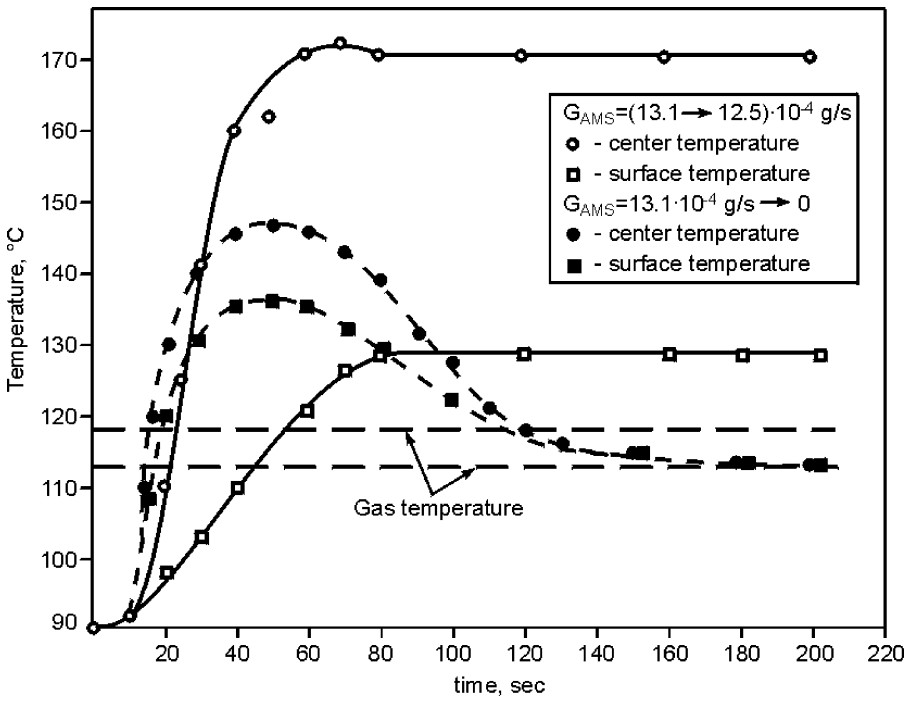

Fig. 11. Impact of the liquid AMS mass flow rate on the transient heat regimes of a catalyst particle. Condition: catalyst 15% Pt/Al_2O_3 with uniform active component distribution, hydrogen flow rate 18.5 cm^3/s.

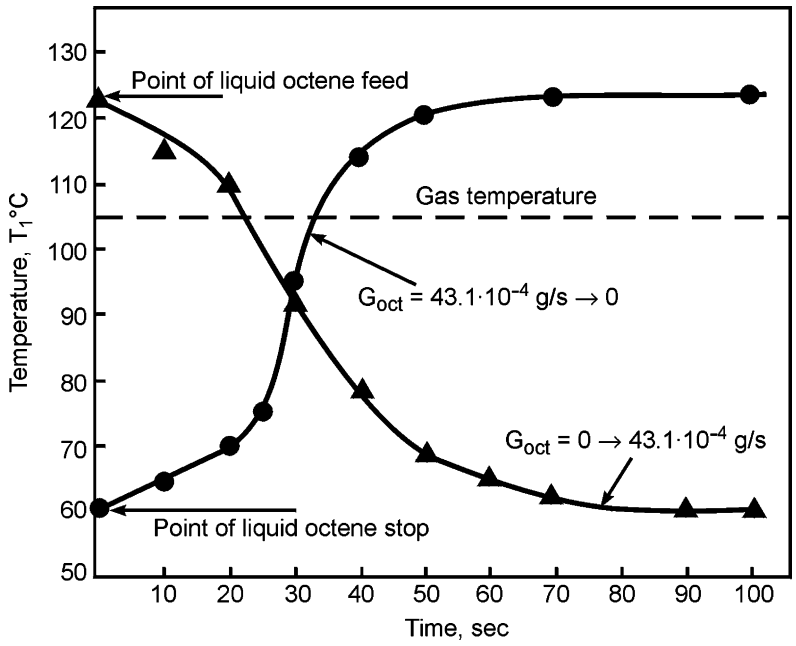

Fig. 12. Transient heat regimes of the particle ignition and liquid filling in the reaction of octene hydrogenation. The octene mole fraction in the gas phase is 0.017, the liquid octene feed is 43.1×10^{-4} g/s, catalyst 15% Pt/Al_2O_3 with uniform active component distribution, hydrogen flow rate 18.5 cm^3/s.

supplied to the particle top, the temperature in the particle was equal to the boiling temperature of octene. After feeding of liquid octene during the particle impregnation, the temperature linearly decreased for 20 s. During this period the porous structure was partially (or completely) filled (the impact of the gas-phase reaction on the heat generation can be neglected), the temperature decreased due to the internal and external evaporation and heat transfer into the bulk. A new steady-state heat regime is attained in 80 s. Due to the contact with liquid and evaporation, the temperature of the particle in this regime is lower than that of gas by 45 °C.

As the liquid feeding is cut off, the temperature in the particle center linearly increases for 25 s. During this time, a part of the porous structure dries and the particle ignition begins. The temperature of the particle center attains the steady-state value during 80 s. This value exceeds the gas temperature by 20 °C as at the starting point of the filling experiments. The total time of the transient regimes in the extinction and ignition experiments (Fig. 12) is very close.

5. Analysis and discussion

The experimental data suggest a rather complex nature of the processes involved in hydrocarbon hydrogenation both on the dry catalyst particle if the reaction proceeds in the region of external diffusion, and partially wetted particle when the chemical reaction is accompanied by liquid evaporation. These results provide the important information concerning the processes of heat and mass transfer during chemical and phase transformations and improve the insight into the mechanism and conditions of appearance of critical phenomena on the catalyst particle, which were discussed in earlier publications [4,11,14–16]. In addition, the above results permit us to estimate coefficients of transfer between a catalyst pellet and a gas flow when the interaction in the multicomponent gas mixture is complicated by liquid evaporation.

5.1. Estimation of mass and heat transfer coefficients

The experimental data presented in Figs. 2–4 show that the hydrocarbon mass transfer to the particle limits the rates of AMS and octene gas-phase hydrogenation under all investigated conditions. On the benzene hydrogenation, this holds only for a narrow temperature range within the maximum particle temperature difference.

For the external mass transfer control, the particle temperature rise is estimated from the following expression [24]:

$$\Delta T = \frac{Qx_A^0}{C_p}\left(\frac{C_p D_0}{\lambda}\frac{P}{RT_0}\right)^{2/3} \quad (1)$$

where $C_p = C_{p_H}x_H^0 + C_{p_A}x_A^0 + C_{p_B}x_B^0$ and D_0 is the effective diffusion coefficient of limiting species at the external diffusion limitation regime. Heat conductivity λ of mixture (H_2+hydrocarbon) is calculated using the empirical method [25] as

$$\lambda = b\lambda_{max} + (1-b)\lambda_{min},$$
$$b = 0.32(1-x_H^0) + 0.8x_H^0, \quad \lambda_{max} = \lambda_A(1-x_H^0) + \lambda_H x_H^0,$$
$$\lambda_{min} = \left[\frac{x_H^0}{\lambda_H} + \frac{1-x_H^0}{\lambda_A}\right]^{-1} \quad (2)$$

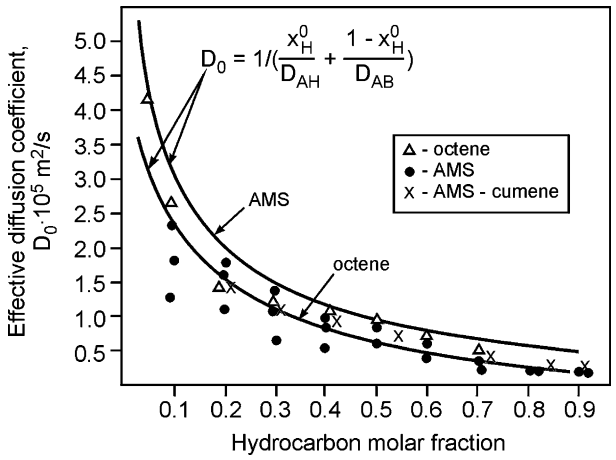

Fig. 13. The effective diffusion coefficient of the limiting component in the reaction of AMS and octene hydrogenation.

These values for the AMS hydrogenation can be estimated from

$$\lambda_H = 0.254 \left(\frac{T}{473}\right)^{1.75} \text{J/m s K},$$

$$\lambda_{AMS} = \lambda_{CUM} = 0.024 \left(\frac{T}{473}\right)^{1.75} \text{J/m s K},$$

$$C_{p_H} = 29 \text{ J/mol K},$$

$$C_{p_{CUM}} = -33.05 + 72.11 \times 10^{-2} T - 3.41 \times 10^{-4} T^2 \text{ J/mol K},$$

$$C_{p_{AMS}} = -8.36 + 0.59T - 2.51 \times 10^{-4} T^2 \text{ J/mol K}$$

Taking into account the experimental values of the particle temperature difference and using formula (2), we can estimate the effective diffusion coefficient for limiting component D_0.

Let us rewrite (1) as

$$D_0 = \left\{\frac{\Delta T C_p}{Q x_A^0}\right\}^{3/2} \frac{\lambda R T_0}{P C_p} \tag{3}$$

Fig. 13 presents D_0 values calculated from the experimental data of Figs. 3 and 4.

For calculation of D_0 a pseudobinary method has been recently developed in [26] and the below formula recommended:

$$\frac{1}{D_0} = \left(\frac{x_H^0}{D_{AH}} + \frac{1 - x_H^0}{D_{AB}}\right) \tag{4}$$

As follows from (4), depending on hydrogen molar fraction x_H^0, the effective diffusion coefficient for the limiting component in the mixture changes from the values corresponding to the binary diffusion coefficient of AMS–H_2 (or octene–H_2) to the binary coefficient for AMS–cumene (or octene–octane). These coefficients for a mixture of AMS–cumene–hydrogen [25] are $D_{AB} = 0.5 \times 10^{-5}(T/473)^{1.9}$ m²/s, $D_{AH} = D_{BH} = 7.5 \times 10^{-5}(T/473)^{1.9}$ m²/s. For the hydrogen–octene–octane mixture, $D_{AB} = 0.4 \times 10^{-5}(T/473)^{1.9}$ m²/s, $D_{AH} = D_{BH} = 6.66 \times 10^{-5}(T/473)^{1.9}$ m²/s. In Fig. 13, the values of D_0, calculated from the formulae (4) are given. One can conclude that the diffusion coefficient calculated by (4) and diffusion experimental values for hydrogenation of AMS and AMS + cumene and octene, calculated from (3), agree well with each other. Thus, one can use formula (4) to calculate ignition of the catalyst pellet and transfer in the external diffusion region during hydrogenation of the multicomponent component as well as coefficients of effective diffusion of the limiting component. For liquid filled catalyst pellet, the rate of the liquid evaporation from the wetted surface into bulk gas may be calculated via equation:

$$W = \beta S \frac{P}{RT_0} M x(T) \quad \text{or} \quad W = \frac{\alpha S M}{H}(T_0 - T) \tag{5}$$

Mass transfer coefficient β in Eq. (5) may be determined from correlation [27]:

$$Sh = 2 + 0.6 Re^{0.5} Sc^{0.33} \tag{6}$$

where $\beta = Sh\, D_0/d$, $Sc = \mu/D_0 \rho_m$, $Re = Ud\rho_m/\mu$ and $\mu = 1.2 \times 10^{-5}(T/473)^{0.75}$.

A mixture of AMS and cumene vapors with hydrogen is a multicomponent system with considerably different binary diffusion coefficients. Therefore, in order to calculate mass transfer coefficients via Eq. (6), one should determine the effective diffusion coefficient for the limiting component in multicomponent mixture. For this purpose we shall use formula (4). For experimental conditions presented in Fig. 10 ($x_{AMS}^0 = 0$ and $T_0 = 119\,^\circ$C), the calculated mass transfer coefficient is $\beta_{AMS} = 0.042$ m/s. In case of cumene evaporation into saturated hydrogen (experimental evidence provided in Fig. 3, $x_{AMS}^0 = 0.3$ and $T_0 = 119\,^\circ$C) $\beta_{CUM} = 0.0075$ m/s.

Other methods to evaluate mass transfer coefficients are based on the experiments with liquid filled catalyst particle exposed to dry or partially saturated hydrogen. Assume that a particle is completely filled and the supplied liquid on the particle to vaporize totally using Eq. (5) and the experimental data of Fig. 6, Fig. 10 one may calculate mass transfer coefficients. The estimated mass transfer coefficient for cumene evaporation (Fig. 6, $G_{CUM} = 10.8 \times 10^{-4}$ g/s) is $\beta_{CUM} = 0.009$ m/s and for AMS evaporation in dry hydrogen (Fig. 10, $G_{AMS} = 18 \times 10^{-4}$ g/s) is 0.037 m/s. These values agree well with the results of calculation by [27].

Convective heat transfer coefficient α can be estimated at correlation similar [27]:

$$Nu = 2 + 0.6 Re^{0.5} Pr^{0.33} \tag{7}$$

where $\alpha = Nu\,\lambda/d$, $Pr = \mu C_p \rho/\lambda\rho_m$, $C_p = x_{H_2}^0 C_{p_{H_2}} + (1 - x_{H_2}^0) C_{p_{AMS}}$.

The calculated value of convective heat transfer coefficient for experimental evidence presented in Fig. 10 ($x_{AMS}^0 = 0$ and $T_0 = 119\,^\circ$C) is 123 W/m² K. Heat transfer coefficient in the case of cumene filled particle (experimental

data presented in Fig. 6, $x^0_{AMS} = 0.3$ and $T_0 = 119\,^\circ C$) is $67\,W/m^2\,K$. Heat transfer coefficient may be estimated also from Eq. (5) and experimental data presented in Figs. 6 and 10. Then we have $\alpha = 171\,W/m^2\,K$ for AMS evaporation into dry hydrogen (Fig. 10, $G_{AMS} = 18 \times 10^{-4}$ g/s, $\Delta T = -30$) and $\alpha = 217\,W/m^2\,K$ for cumene evaporation into the AMS-saturated hydrogen (Fig. 6, $G_{CUM} = 10.8 \times 10^{-4}$ g/s, $\Delta T = -12$). Thus calculated heat transfer coefficients are similar to each other, but considerably differ from the calculated convective heat transfer coefficients. This result shows essential impact of evaporation on heat transfer between gas and liquid filled catalyst pellet.

5.2. Estimation of heat regimes at the low hysteresis branch

Let us assume that a particle is isothermal and partially wetted or completely filled; the wetted particle area fraction is characterized by factor f; hydrogenation in the liquid phase is negligible; the gas-phase reaction proceeds over the unwetted catalyst surface between hydrogen and AMS vapor which diffuses after evaporation from the gas–liquid surface into the porous structure; AMS evaporates into the bulk gas from the particle-wetted surface. According to [28], the activation energy of AMS hydrogenation is $E \approx 43\,500$ J/mol, the rate of gas-phase reaction depends on hydrogen concentration to power 0.8 and is almost insensitive to the AMS vapor concentration [1]. Assuming that there is no mass transfer limitation of the gas-phase reaction with respect to hydrogen, the heat and mass balance equations can be written as

$$K_0\eta \exp\left(-\frac{E}{RT}\right)(x^0_H)^{0.8}(Q-H)(1-f) + \alpha(T_0 - T) - \beta_{AMS}\frac{P}{RT_0}fHx_{AMS} = 0 \quad (8)$$

$$G_{AMS} = \beta_{AMS}\frac{P}{RT_0}SM_{AMS}fx_{AMS} + K_0\eta \exp \times \left(-\frac{E}{RT}\right)(x^0_H)^{0.8}(1-f)SM_{AMS} \quad (9)$$

Taking into account the approximation [24] $\exp(-E/RT) \approx \exp(-E/RT_0)\exp\theta$, introducing new dimensionless temperature $\theta = (T - T_0)E/RT_0^2$, and assuming $x_{AMS} = C_{AMS}P_{AMS}(T)/P = C_{AMS}P_{AMS}(T_0)/P\exp((H/E)\theta),$, Eqs. (8) and (9) can be rewritten as

$$\delta \exp\theta(1-f) - \theta - \Lambda f \exp\left(\frac{H}{E}\theta\right) = 0 \quad (10)$$

$$\gamma \exp\left(-\frac{H}{E}\theta\right) - f - \chi(1-f)\exp\left[\left(1-\frac{H}{E}\right)\theta\right] = 0 \quad (11)$$

where

$$\delta = \frac{K_0\eta(Q-H)\exp(-E/RT_0)}{\alpha}\frac{E}{RT_0^2},$$

$$\Lambda = \frac{\beta_{AMS}H}{\alpha}\frac{P_{AMS}(T_0)}{RT_0}\frac{E}{RT_0^2}C_{AMS}, \qquad \chi = \frac{\delta}{\Lambda}\frac{H}{Q-H},$$

$$\gamma = \frac{G_{AMS}}{\beta_{AMS}(P_{AMS}(T_0)/RT_0)SM_{AMS}C_{AMS}}, \qquad x^0_{H_2} = 1$$

The dimensionless variables in Eqs. (10) and (11) are determined for the gas bulk conditions and characterize: δ—the ratio between the heat generation in the chemical reaction and the convective heat removal from the particle surface; Λ—the ratio between the liquid evaporation heat and the convective heat removal from the particle surface; χ—the ratio between the rate of chemical reaction and the rate of liquid vaporization; γ—the ratio between the liquid mass flow rate and the liquid vaporization rate. The mass transfer coefficient $\beta_{AMS} = 0.042$ m/s and heat transfer coefficient $\alpha = 123\,W/m^2\,K$ were calculated from the correlation (6, 7).

From (10) and (11) one can obtain the temperature transcendental equation and the equation for the wetted area fraction f:

$$\frac{(\delta + \Lambda\chi)\exp\theta - \Lambda\gamma - \delta\gamma\exp((1-H/E)\theta)}{1 - \chi\exp((1-H/E)\theta)} - \theta = 0 \quad (12)$$

$$f = \gamma\exp\left(-\frac{H}{E}\theta\right)\frac{1-(\chi/\gamma)\exp\theta}{1-\chi\exp((1-H/E)\theta)} \quad (13)$$

As follow from (12) and (13), $\theta = -\Lambda\gamma$, $f = \gamma\exp(-(H/E)\theta)$ if $\delta = 0$ and $\chi = 0$.

This means that the heat transferred from the bulk is spent to vaporize the liquid. Therefore, the particle temperature is lower than the gas bulk temperature. From the experimental data in Fig. 10, one can calculate θ, γ and δ and use Eq. (13) to estimate f. The obtained results are presented in Fig. 14. The dots correspond to the fraction of wetted surface calculated using formula (13) from the experimental data in Fig. 10. It is seen that the fraction of the wetted surface depends on the rate of liquid mass flow supplied to a catalyst particle, the gas temperature and types of catalyst. The effect of the liquid flow rate on the wetted area fraction has been already reported in the literature [29]. However, the impact of the gas temperature and, consequently, the catalyst temperature and active component distribution in the particle on the wetted area fraction in the hydrogenation reaction was demonstrated for the first time.

Eq. (12) is transcendental with respect to θ and describes the dependence of temperature of the catalyst particle on parameters of the mathematical model. In order to determine the conditions of the catalyst particle ignition (the experimental conditions are shown in shown in Fig. 10), one should determine the bifurcation points of function $\theta(\gamma)$. To calculate these coordinates, it is necessary to differentiate

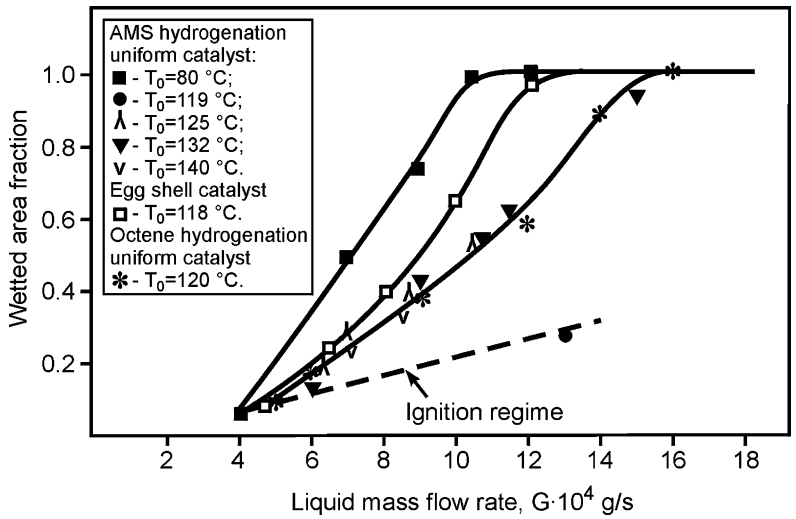

Fig. 14. Impact of the liquid AMS mass flow rate and the gas temperature on the wetted area fraction on the low-temperature hysteresis branch. Parameters for calculations by Eq. (13) are $Q = 116\,000$ J/mol, $E = 43\,500$ J/mol, $E/H = 1.1$. $T_0 = 80\,^{\circ}$C: $\Lambda = 1.54$, $\delta = 0.7$; regenerated catalyst $T_0 = 119\,^{\circ}$C: $\Lambda = 3.52$, $\delta = 5$; $T_0 = 125\,^{\circ}$C: $\Lambda = 0.78$, $\delta = 0.35$; $T_0 = 132\,^{\circ}$C: $\Lambda = 4.47$, $\delta = 0.9$; egg-shell catalyst $T_0 = 118\,^{\circ}$C: $\Lambda = 3.52$, $\delta = 1.16$.

Eq. (12) with respect to θ and then assume $d\gamma/d\theta = 0$. Finally we have

$$(\delta + \Lambda\chi)\exp\theta^x + \exp\left[\left(1 - \frac{H}{E}\right)\theta^x\right] \times \left[\chi + \left(1 - \frac{H}{E}\right)(\theta^x\chi - \delta\gamma^x)\right] = 1 \quad (14)$$

Since Eq. (14) is transcendental with respect to θ^x, we can use it do determine $\gamma(\theta^x)$. According to the numerical analysis of this function, if the value of evaporation heat is higher than the energy of reaction activation, then $\gamma^x > 0$ if $\theta^x > 0$. By this is meant that ignition of the partially wetted particles will not occur if $E/H < 1$. In Fig. 15, we illustrate the case when $E/H > 1$. Solid lines correspond to calculations $\gamma(\theta^x)$ at different δ, the shaded region determines the experimental conditions at which a catalyst particle was presumably ignited on the lower branch of the hysteresis curve given in Fig. 10. The figure suggests that the critical conditions of the catalyst particle ignition depend on the relation between heat evolved from the reaction and the intensity of heat removal from the catalyst particle determined by parameter δ. The other important parameter, which significantly affects ignition, is the relation between the amount of liquid supplied to the particle and the rate of its evaporation. It should be noted that for the runaway conditions, the fraction of wetted surface, calculated from Eq. (13), varies from 0.05 to 0.24 (Fig. 14, dotted line).

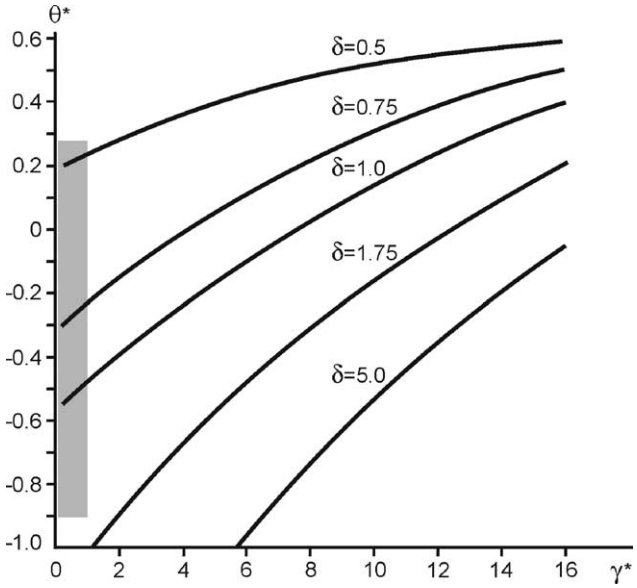

Fig. 15. Impact of parameters δ and γ^* on the particle ignition condition at the low-temperature steady-state regime. A continuous line shows the results calculated by Eq. (13), the shaded area is the experimental ignition field.

6. Conclusions

Steady-state and dynamic-heat regimes on the dry, partially wetted, and completely filled catalyst particles were studied using the model reactions of benzene, AMS and octene hydrogenation over the several catalysts with different porous structures, apparent catalytic activities, and heat conductivities. A rise in the particle temperature at the external limitation regime was studied and the effective diffusion coefficients of limiting species were determined. For this purpose we varied the following parameters: particle preheating regime, gas temperature, hydrogen saturation of AMS or octene vapors, and liquid mass flow rate on the top of a catalyst particle.

We have studied experimentally steady-state and dynamic-heat regimes on partially wetted and completely filled

catalyst particles. The experiments on the single catalyst particle demonstrated a strong temperature gradient in the particle at the drying and filling regimes. We have estimated the impact of phase equilibrium between the saturated hydrogen and the partially wetted catalyst particle and the phase transition on the particle runaway. Evaporation of the liquid over the external catalyst surface and the liquid filling the particle porous structure result in the formation of two stable steady states of the catalytic particle at certain rates of liquid flow. It was found that there is a strong dependence between such parameters as particle temperature, wetted area fraction, critical liquid flow rates, providing the ignition and liquid filling, hydrocarbon vapor fraction in the gas phase, and gas temperature, apparent catalytic activity, and thermal conductivity of catalysts. We have estimated the external wetted area fraction, mass and heat transfer coefficients, and the filling and ignition conditions at these regimes with respect to the gas temperature, the particle heat conductivity and the rate of liquid feeding onto the particle.

Acknowledgements

The authors gratefully acknowledge the financial support of The Netherlands Organization for Scientific Research (NWO) under grants 047-011-000-01 and 047-014-004, and Dr. A.E. Kronberg and Prof. K.R. Westerterp for fruitful discussion of this research.

References

[1] A.H. Germain, A.G. Lefebvre, G.A. L'Homme, Experimental study of a catalyst trickle-bed reactor, Adv. Chem. Ser. 133 (1974) 164–180.
[2] S.B. Jaffe, Hot spot simulation in commercial hydrogenation processes, Ind. Eng. Chem. Proc. Des. Dev. 15 (3) (1976) 410–416.
[3] J. Hanika, K. Sporka, V. Ruzicka, J. Hrstka, Measurement of axial temperature profiles in an adiabatic trickle bed reactor, The Chem. Eng. J. 12 (1976) 193–197.
[4] J. Hanika, J. Ruzicka, Modeling of a trickle bed with strong exothermal reaction, Catal. Today 24 (1995) 87–93.
[5] R.L. McManus, A.G. Funk, P. Harold, K.M. Ng, Experimental study of reaction in trickle bed reactors with liquid maldistribution, Ind. Eng. Chem. Res. 32 (1993) 570–576.
[6] J. Hanika, V. Stanek, Design and Operation of Trickle-bed Reactors, Handbook of Heat and Mass Transfer, vol. 2, Gulf Publishing Co., Houston, 1986, pp. 1029–1080.
[7] J. Růžička, J. Hanika, Partial wetting and forced reaction mixture transition in a model trickle-bed reactor, Catal. Today 20 (1994) 467–484.
[8] V.A. Kirillov, Gas Liquid–Solid Reactors with Cocurrent Up- and Down Flow Operation, Siberian Branch of the Russian Academy of Sciences, Novosibirsk, 1997 (in Russian).
[9] G. Eigenberger, U. Wegerle, Runaway in an industrial hydrogenation reactor, in: Proceedings of the Chemical Reaction Engineering Symposium, vol. 133, Boston, Amer. Chem. Soc., 1982, pp. 133–148.
[10] E. Goossens, R. Donker, F. Van den Brink, Reactor runaway in pyrolysis gasoline hydrogenation, in: Proceedings of the First International Symposium on Hydrotreatment and Hydrocracking of Oil Fraction, Oostende, Belgium, February 17–19, 1997.
[11] G.A. Funk, M.P. Harold, K.M. Ng, Experimental study of reaction in a partially wetted catalytic particle, AIChE J. 37 (2) (1991) 202–214.
[12] C.N. Satterfield, F. Ozel, Direct solid-catalyzed reaction of a vapor in an apparently completely wetted trickle-bed reactor, AIChE J. 19 (1973) 1259–1263.
[13] W. Sedriks, C.N. Kenney, Partial wetting in trickle-bed reactors—the reduction of crotonaldehyde over a palladium catalyst, Chem. Eng. Sci. 28 (1973) 559–568.
[14] P.C. Watson, M.P. Harold, Dynamic effects of vaporization with exothermic reaction in a porous catalytic particle, AIChE J. 39 (1993) 989–1006.
[15] P.C. Watson, M.P. Harold, Rate enhancement and multiplicity in a partially wetted and filled particle: experimental study, AIChE J. 40 (1994) 97–111.
[16] A.V. Kulikov, N.A. Kuzin, A.B. Shigarov, V.A. Kirillov, A.E. Kronberg, K.R. Westerterp, Experimental study of vaporization effect on steady state and dynamic behavior of catalyst particles, Catal. Today 66 (2001) 255–262.
[17] A.B. Shigarov, A.V. Kulikov, N.A. Kuzin, V.A. Kirillov, Modeling of critical phenomena for liquid/vapor–gas exothermic reaction on single catalyst pellet, Chem. Eng. J. 4069 (2002) 1–9.
[18] V.A. Kirillov, I.A. Mikhailova, S.I. Fadeev, V.K. Korolev, Study of the critical phenomena in exothermic catalytic reaction on the single partially-wetted porous catalyst particle, Combust. Explos. Shook Wales 38 (2002) 22–32.
[19] N.Ya. Buben, Heat regime of the Pt wire in the reaction of hydrogen and ammonia oxidation, J. Phys. Chem. Additional Volume (1946) 123–128 (in Russian).
[20] V.I. Lugovskoi, Yu.Sh. Matros, V.A. Kirillov, M.G. Slin'ko, Investigation of the runaway porous catalyst particle, Theor. Foundation Chem. Eng. 8 (4) (1974) 616–618 (in Russian).
[21] R.R. Graham, F.C. Vidaurri, A.J. Gully, Catalytic dehydrogenation of cyclohexane: a transparent controlled model, AIChE J. 14 (3) (1968) 473–479.
[22] A.B. Shigarov, S.I. Fadeev, I.A. Mikhailova, A.V. Kulikov, V.K. Korolev, N.A. Kuzin, V.A. Kirillov, Simplified treatment of mass transfer for gas-phase hydrogenation/dehydrogenation of heavy compounds, Kor. J. Chem. Eng. 19 (2) (2002) 252–260.
[23] N.M. Ostrovskii, A. Parmaliana, F. Frusteri, L.P. Maslova, N. Jiordano, Investigation of the benzene hydrogenation on the monolith Pt/Al_2O_3 catalyst, Kinet. Katal. 32 (1991) 78–84 (in Russian).
[24] D.A. Frank Kamenetzki, Diffusion and Heat Transfer in Chemical Kinetics, Nauka, Moscow, 1987 (in Russian).
[25] R.C. Reid, J.M. Prausnitz, Properties of Gases and Liquid, McGraw-Hill, New York, 1977.
[26] V.A. Kirillov, N.A. Kuzin, A.V. Kulikov, B.N. Luk'janov, V.M. Khanaev, A.B. Shigarov, Investigation of the gas phase hydrocarbon hydrogenation on a single catalyst particle at the external mass transfer limitation, Theor. Foundation Chem. Eng. 34 (5) (2000) 526–536 (in Russian).
[27] G.A. Hugmark, Mass and heat transfer from rigid spheres, AIChE J. 13 (1967) 1219–2130.
[28] P. Cini, M.P. Harold, Experimental study of the tubular multiphase catalyst, AIChE J. 37 (7) (1991) 997.
[29] M.H. Al-Dahhan, M.P. Dudukovic, Catalyst wetting efficiency in trickle bed reactors at high pressure, Chem. Eng. Sci. 50 (1995) 2377–2389.